A medium energy ion scattering and x-ray photoelectron spectroscopy study of physical vapor deposited thin cerium oxide films on Si(100)

R. Barnes, D. Starodub,[b] and T. Gustafsson[c]
Department of Physics and Astronomy, and Laboratory for Surface Modification, Rutgers, The State University of New Jersey, 136 Frelinghuysen Road, Piscataway, New Jersey 08854-8019

E. Garfunkel
Department of Chemistry and Chemical Biology, and Laboratory for Surface Modification, Rutgers, The State University of New Jersey, 136 Frelinghuysen Road, Piscataway, New Jersey 08854-8019

(Received 3 January 2006; accepted 23 June 2006; published online 17 August 2006)

40 Å thick cerium oxide films have been grown on Si(100) substrates via physical vapor deposition of cerium metal in an oxygen background. The films have been characterized for their composition and thermal properties upon deposition and under different annealing conditions via x-ray photoelectron spectroscopy and medium energy ion scattering (MEIS) and their morphology using atomic force microscopy. By reoxidizing the films in $^{18}O_2$ gas and using MEIS, we investigated the processes responsible for film formation. We found that annealing the as-deposited samples to 750 °C produced a cerium silicate film with a sharp silicate:silicon interface. Our results show that the oxygen transport in both the oxide and silicate films occurs via an exchange mechanism. © *2006 American Institute of Physics*. [DOI: 10.1063/1.2234820]

I. INTRODUCTION

There is considerable interest in using metal oxides for devices, in particular, as alternative dielectrics for aggressively scaled complementary metal oxide semiconductor (CMOS) applications.[1,2] CeO_2 has a high dielectric constant and is chemically stable on silicon,[3] which makes it a good candidate as an alternate gate dielectric. The dielectric constant for amorphous CeO_2 is ~15,[1] for polycrystalline CeO_2 ~26,[1] and for single-crystal ceria films on Si(111) as high as 52.[4] The close CeO_2–Si lattice match makes it a candidate material for heteroepitaxial growth of single-crystal films or for a buffer layer in gate stacks. In particular, CeO_2 (100)-oriented films may be considered for use as a buffer layer between perovskite structures and silicon,[5,6] and (111)-oriented CeO_2 films as buffer layers in metal ferroelectric insulator semiconductor (MFIS) structures.[7] Cerium silicate is under investigation for use in blue/violet light-emitting devices,[8,9] as well.

Since cerium oxide films are attractive candidates for a diverse set of applications, it is necessary to understand the processes that lead to their formation, composition, and behavior under conditions characteristic of device processing, i.e., their evolution upon annealing. The presence of two cerium valence states, Ce III and Ce IV, is a nontrivial complication. Hirschauer *et al.* have studied CeO_2 films on Si(111). They report a complex film composition, containing silicon oxide, a mixed Ce:Si:O layer, and at least two cerium oxides.[9] The behavior of these interfaces during annealing, particularly the mechanisms of oxidation and reduction for silicon in contact with cerium, and the evolution of the film composition are not well understood.[10,11]

Epitaxial CeO_2 films have been grown on Si(111);[4,12,13] however, the task of growing single-crystal cerium oxide films on the (more important for commercial applications) Si(100) surface has been proven challenging. The difficulty is partly due to the behavior of oxygen at the film-substrate interface. There are a number of possible crystal orientations for CeO_2 at the Si(100) surface, and the resulting films are often polycrystalline.[12,14,15] Oxygen presence during film deposition has here an important influence on crystallinity and orientation:[16–18] the background oxygen pressure and the presence of an amorphous interface during deposition particularly affect the film growth and crystalline direction.[17] The elimination of an amorphous interface is also an issue,[4,13,14,19] as an insulator's usefulness in a silicon-based device depends on the sharpness of the silicon/insulator transition. SiO_x forms at the ceria/silicon interface under some conditions, and the SiO_2 and CeO_2 should interact and form mixed phases, unlike Si and CeO_2. Si oxidation in the presence of Ce is complicated. Ce is known to catalyze the oxidation of Si(111) (Ref. 20) and Si(100),[21] a process thought to be a consequence of cerium's two valence states, Ce III and Ce IV.[22] Although formation of single-crystal CeO_2(110) over Si(100) has been reported,[23,24] a better understanding of the ceria/silicon interface is clearly needed.

We have deposited cerium oxide films by evaporating cerium metal in an oxygen background on native-oxide-covered Si(100); we use oxide-covered Si(100) so that the surface is well controlled in the presence of gas-phase oxygen. We studied their behavior upon annealing in vacuum as well as after reoxidation in an $^{18}O_2$ background. We have characterized the samples using x-ray photoelectron spectroscopy (XPS) and medium energy ion scattering (MEIS).

[a]Present address: Department of Chemistry, University of Washington, Box 351700, Seattle, Washington 98195-1700.
[b]Present address: Department of Physics and Astronomy, Arizona State University, P.O. Box 871504, Tempe, Arizona 85287-1504.
[c]Electronic mail: gustaf@physics.rutgers.edu

We also looked at the sample morphology with atomic force microscopy (AFM) before and after annealing.

II. EXPERIMENT

Films were deposited by electron beam evaporation of cerium metal in an oxygen background onto Si(100) substrates covered with ~10 Å of native oxide. The substrates were prepared by cleaning with methanol and heating in vacuum for several hours at 300 °C to remove organic contamination. The base pressure in the deposition chamber was 1.0×10^{-9} Torr, and the e-beam source background due to outgassing during deposition was 5×10^{-8} Torr. All of the samples were deposited at room temperature in an oxygen background of 6.6×10^{-6} Torr over 10 min time, using a cerium metal evaporator that was built in-house and similar to that described by Beag *et al.*[25] We performed XPS measurements *in situ* on the as-deposited films to determine cleanliness, oxidation state, and thickness using a Kratos XSAM 800 surface analysis system. For these measurements, we use a Mg $K\alpha$ source. The samples were then transferred through air for MEIS or AFM analysis; for the latter we used a Quesant Q-Scope 250 AFM in noncontact mode.

MEIS is a low-energy, high resolution version of conventional Rutherford backscattering spectroscopy (RBS). By using a lower ion beam energy (130.8 keV protons for the present experiments) it is possible to replace the medium resolution semiconductor detectors used in RBS with a high resolution electrostatic ion energy analyzer. The ion-solid interaction follows classical scattering, just as in RBS, making quantitative analysis possible. The incident ions lose energy primarily to electronic excitations (including ionization) as they travel through the sample; from the averaged energy loss, we extract information about the depth distribution of the target elements. Under favorable conditions, the depth resolution is ~3 Å at the outer surface.[26,27]

The ion beam was aligned along the [100] direction of the Si substrate, resulting in a much reduced signal from the substrate and making detailed analysis of the weak oxygen signal possible. The energy spectra from protons scattered in the (110) plane were collected simultaneously in an angular range of 20° with an angular resolution of 0.2°, centered around a 128° scattering angle.[28] Unless otherwise noted, all MEIS spectra presented below correspond to a scattering angle of 125°. This corresponds to a double alignment geometry in the substrate, further reducing the background substrate signal. To obtain a depth profile, we compute the energy spectra for tentative model structures and vary them until the best agreement between the calculated and experimental spectra is obtained. For the calculation, we use a screened Coulomb potential (the Moliére potential,[29] a numerical approximation to the Thomas-Fermi potential) to model the scattering cross section. The elemental stopping powers are given by semiempirical literature values.[30] To account for straggling (a broadening of the energy spectrum due to statistical fluctuations in the interactions between the incident beam and the target electrons), we assign a Gaussian form to the simulated scattering signal; this Gaussian has a standard deviation numerically derived[31] and empirically fitted[32] using the Hartree-Fock-Slater electronic charge distribution and taking into account correlation effects. The stopping power and straggling in a compound have been determined from elemental values using Bragg's summation rule. The interaction between proton and target is completely described within this framework, leaving film thickness and composition as the only fitting parameters in the model.

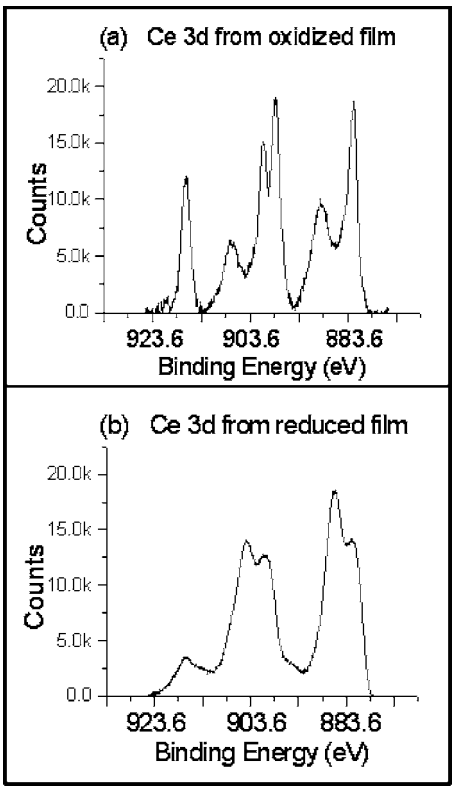

FIG. 1. Ce 3*d* XPS spectra (after linear background subtraction) from cerium oxide showing (a) mostly Ce^{4+} character and (b) mostly Ce^{3+} character.

III. RESULTS AND DISCUSSION

A. Structure and composition of ceria films

Cerium oxide has a complex cerium core photoelectron structure. The Ce 3*d* core level high resolution spectrum contains a minimum of ten peaks, four attributed to the Ce^{3+} valence state and six due to the Ce^{4+} valence state. These peaks arise from $3d_{5/2}$-$3d_{3/2}$ spin orbit splitting combined with possible $4f^0$, $4f^1$, and $4f^2$ final states; the peak assignments are discussed in detail in the literature.[11,33–35] Figure 1 shows a medium resolution Ce 3*d* spectrum from a highly oxidized cerium oxide film and from a mostly reduced cerium oxide film. The predominant features in Fig. 1(a) belong to the 4+ valence state, and Fig. 1(b) contains features characteristic of the 3+ valence state; the spectra are clearly different from one another. Since each of the peaks in the Ce 3*d* spectrum is distinct, it provides an ideal tool for determining the average oxidation state of the film.

To quantify the XPS data, we used methods similar to those described by Preisler *et al.*,[11] who determined the oxidation state of their cerium oxide on silicon samples by fitting core level spectra, including Ce 3*d* and Si 2*p*. Here, we use a linear background subtraction for our medium resolu-

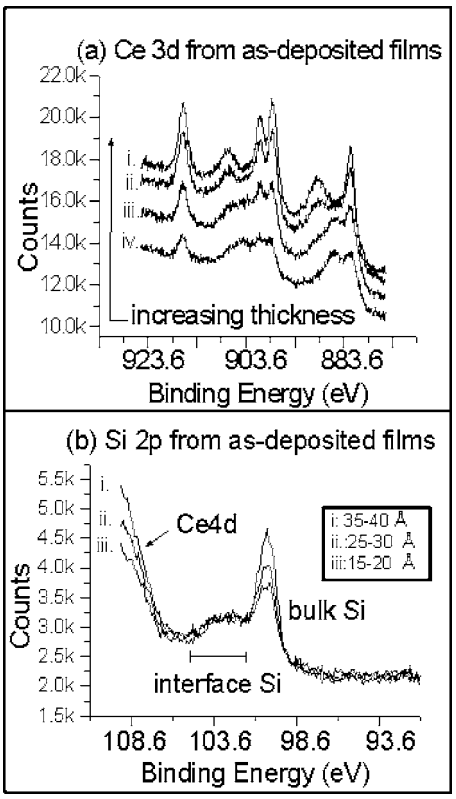

FIG. 2. XPS spectra from three films of varying thickness, deposited with similar oxygen exposure: 6.6×10^{-6} Torr O_2 for 10 min. (a) Ce 3*d* spectra showing progressively decreasing Ce^{4+} character as the film gets thinner. (b) Si 2*p* spectra showing similar interface signals for the three sample thicknesses.

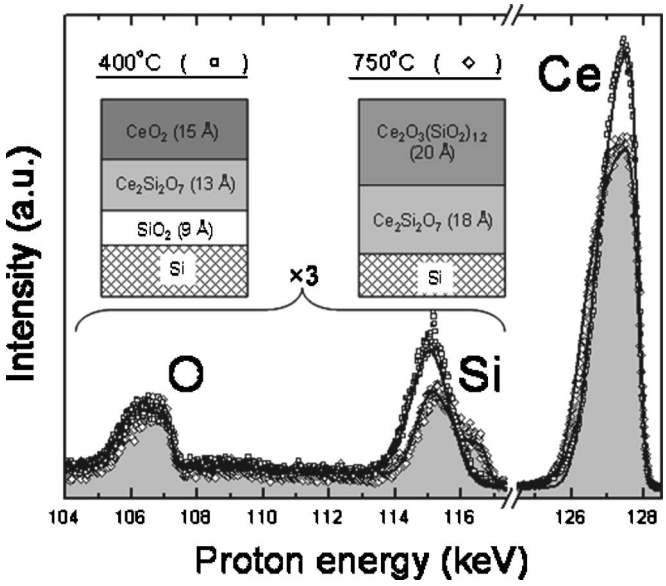

FIG. 3. MEIS energy spectra for ceria films annealed at 400 °C (squares) and 750 °C (diamonds). The solid lines show simulated spectra obtained using model structures sketched in the inset.

tion Ce 3*d* and Si 2*p* spectra and fit the data with Gaussian peaks corresponding to core level shifts associated with the relevant oxidation states. The relative weights of the peaks from the best fits then give an estimation of the valence content of the films. To determine the film thickness upon deposition, we used the peak-to-peak ratios of the Ce 4*d* signal to that of the bulk Si 2*p* signal. Figure 2 contains raw Ce 3*d* and Si 2*p* spectra for several film thicknesses, each deposited under similar oxygen exposure: 6.6×10^{-6} Torr over 10 min. The thickest film is labeled "i." and has a Ce 3*d* spectrum consistent with the highly oxidized spectrum in Fig. 1(a). The thinner films "ii." and "iii." are consistent with a superposition of features from Figs. 1(a) and 1(b). The thinnest film in Fig. 2(a) exhibits Ce^{3+} character more prominently, as seen in spectrum "iv.," which was obtained from a very thin (<15 Å) oxide film. The average oxidation state for the samples contains progressively more Ce^{3+} character as the films are deposited more thinly. This is consistent with a layer of Ce^{3+} species being deposited at the substrate/film interface, and that layer being covered by a slab containing Ce^{4+} species. Figure 2(b) contains the raw Si 2*p* spectra for the three films i., ii., and iii.; the spectra are similar for all three thicknesses and provide no evidence for differences in the interface structure. However, the Si 2*p* signals from the interface are shifted in energy relative to the bulk Si signal, indicating that they contain Si^{3+} species, likely from an interface silicate, and Si^{4+} from SiO_2. From these data we conclude that upon deposition we create a ternary oxide interface containing Ce and Si species with primarily 3+ valence. The remaining deposited oxide primarily contains the fully oxidized, Ce^{4+} species found in CeO_2.

The MEIS energy spectra in Fig. 3 compare films, similar in thickness and deposited under like conditions, which were subsequently annealed in ultrahigh vacuum (UHV) at 400 and 750 °C for several minutes. The former showed no noticeable change compared to the as-deposited film. For MEIS fitting and analysis of the film annealed at 400 °C, we model the film structure with a multilayer system assuming the presence of both Ce^{3+} and Ce^{4+} species and that the deposited film has the layered slab structure of bulk $Si:SiO_2:Ce_2Si_2O_7:CeO_2$. As described above, we attribute the Ce^{4+} to a fully oxidized top layer that exists atop of a slab of cerium pyrosilicate, $Ce_2Si_2O_7$. The CeO_2 layer thickness was the single parameter varied, and the remaining Ce, determined from the Ce peak area in the MEIS spectrum, is ascribed to the submerged pyrosilicate layer. We must introduce an interfacial layer of SiO_2 to the model to account for extra oxygen. The best fit to the measured MEIS spectrum gave CeO_2, $Ce_2Si_2O_7$, and SiO_2 thicknesses of 15, 13, and 9 Å, respectively, in good agreement with XPS estimates. Annealing to 750 °C produced two additional features in the spectrum characteristic of phase mixing: a distinct shoulder on the high-energy side of the Si peak and a broadening of the Ce peak. The shoulder on the Si peak indicates that there is some Si near the surface of the sample, which could be due to a void formation in the film or Si diffusing from the interface to the surface. Consideration of the Ce peak shape argues against a void formation model: if a void was exposing the substrate Si the width of the Ce peak should remain unchanged, with only its height affected. Instead, the Ce peak broadens (corresponding to a Ce distribution over a larger depth). In addition (see below) AFM shows that the surface remains flat. Together with the appearance of the high-energy Si shoulder, these observations imply Si out-

diffusion toward the surface at 750 °C, consistent with mixing. Because the heating was performed in UHV, we expect that all Ce in the film takes the form of a Ce^{3+} species after the high-temperature annealing, since reduction of the Ce^{4+} state to the Ce^{3+} suboxide via Si oxidation is thermodynamically allowed. We introduce the oxygen deficient silicate $Ce_2O_3(SiO_2)_x$ with $x \leqslant 2$ to the model used for simulating the energy spectra. We varied the thickness of this layer and stoichiometric coefficient x, and the best agreement between the calculated and experimental spectra was obtained by using $x=1.2$, a thickness of the top $Ce_2O_3(SiO_2)_{1.2}$ layer of 20 Å, and a thickness of the underlying $Ce_2Si_2O_7$ of 18 Å. Our best fits show that there was no interfacial silicon oxide layer in these annealed samples and that the interface with the Si substrate was sharp. Upon heating the samples to higher temperatures, the film remains stable during prolonged annealing at 820 °C, but increasing the temperature to 850 °C leads to film decomposition. The corresponding MEIS energy spectrum (not shown) is characterized by a broad and low Ce peak (implying Ce distributed over a greater depth) and a sharp surface Si peak with long low-energy tail mimicking that of the Ce peak. All oxygen is removed from the film. We attribute these observations to the formation of Ce silicide islands on a clean Si surface (as has been observed for many metal oxide on Si systems annealed in vacuum to high temperature).[36,37] Our AFM measurements indicate that both oxide and silicate films are flat upon deposition with a rms roughness of 1.5–2.2 Å. The films annealed to 750 °C remained flat, but those that were heated above 850 °C were rough, with a rms value of approximately 100 Å.

In summary, these samples present a possible opportunity: the MEIS spectra here indicate that annealing in vacuum produces a complex but uniform cerium silicate film that does not contain a pure SiO_2 layer at the interface existing in the as-grown films. We suggest that it is possible to control the available oxygen in these samples, for example, by thermal oxidation of a Si substrate prior to Ce deposition or by controlling background oxygen pressure during deposition, to allow for precise oxygen content in the film. This could produce a SiO_2-free interface while making possible fine tuning of the final film stoichiometry upon annealing to produce desirable compositional and electrical properties for engineering applications. The driving thermodynamics of this multilayer system and the kinetics controlling which (multilayer) metastable phase structures will be reached will be very condition dependent.

B. Oxygen isotopic substitution and transport

To gain a better understanding of the oxygen transport properties, we reoxidized samples in $^{18}O_2$ gas. A first sample was annealed in UHV to 750 °C to convert the as-deposited cerium oxide film into a cerium silicate as described above. This film was then reoxidized in $^{18}O_2$ gas at 500 °C and 10^{-2} Torr $^{18}O_2$ for 15 min. Figure 4(a) shows the MEIS energy spectra from the film before and after treatment. The change in the Ce peak is negligibly small, indicating that the Ce distribution does not change upon annealing. There are,

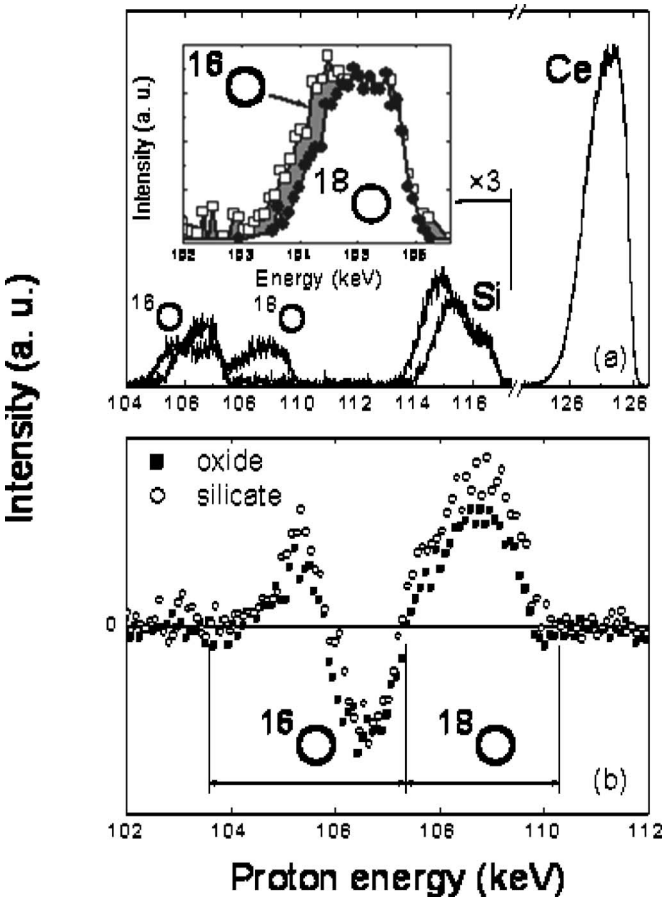

FIG. 4. The upper graph shows MEIS energy spectra from the cerium silicate film before and after reoxidation in $^{18}O_2$. The inset shows the ^{18}O peak superimposed on the ^{16}O peak in the same spectrum by shifting its energy position by the known difference in scattered energy. The scattering angle was 133°. The lower graph shows a difference spectra in the oxygen energy region for the films annealed at 400 °C (filled squares) and 750 °C (open circles).

however, several dramatic changes in the oxygen region of the spectra: (1) a large ^{18}O peak appears, indicating significant oxygen incorporation into the film during reoxidation, and (2) the ^{16}O peak becomes lower and broader. The second observation combined with a similar increase in the Si peak width (0.5 keV) and area means that interfacial SiO_2 growth has occurred. The SiO_2 thickness can be estimated easily either from the Si and O peak width increase (assuming a proton stopping power in the SiO_2 matrix of 11.6 eV/Å)[38] or from the increase of the Si and total ($^{16}O+^{18}O$) oxygen signal (assuming a SiO_2 density of 2.19 g/cm^3). Both methods imply the formation of a 14–16 Å thick SiO_2 interface, confirmed by explicitly fitting the spectra. The measured ratio of visible Si increase to that of O of 1:2.13 is quite close to the 1:2 stoichiometry for silica. From this we conclude that the overall oxygen incorporation in the film is primarily due to an interface reaction with Si. The oxygen gain can be attributed mostly to the formation of interfacial Si oxide, but ^{18}O is clearly present in the bulk of the silicate film; the reaction in the bulk of the ceria film is mostly limited to the substitution of network ^{16}O by ^{18}O, arriving from the gas phase. The increase of the oxygen concentration in the silicate layer would result in a smaller ratio of the increase of visible Si to

that of O. The observed interfacial oxide thickness here is much higher than that obtained during reoxidation of ZrO_2 oxide films fabricated on Si(100),[39] where a similar amount of SiO_2 was obtained only after exposure to oxygen at much higher pressure (1 Torr) and higher temperature. The difference is even more striking if we compare the behavior of ceria films to the behavior of hafnium oxide and silicate films under similar oxidation conditions. In the latter system, interaction with oxygen is dominated by an exchange reaction in the bulk of the film with loss of the originally present oxygen into the gas phase without an interfacial reaction with the substrate or overall oxygen uptake.[40] On the contrary, in cerium silicate films, the oxygen uptake prevails over exchange with the gas phase. In particular, we observe an oxygen uptake resulting from $^{18}O_2$ annealing of 6.4×10^{15} cm^{-2} (this gain constitutes 40% of the original oxygen concentration in the film), while the ^{16}O loss into the gas phase was measured to be only 1.9×10^{15} cm^{-2} (12%). The enhanced growth rate of interfacial SiO_2 in the case of cerium-based films can be explained by the well-known fact that the presence of Ce readily promotes Si oxidation by reduction of Ce^{4+} to the Ce^{3+} state. Ce^{4+} can be formed from Ce^{3+} in the silicate by reaction with oxygen from the gas phase. To compare the O isotopic distributions after reoxidation, in the inset to Fig. 4(a) we superimpose the ^{18}O peak on the ^{16}O peak. The former is shifted relative to its actual position by a value, defined by the difference between the ^{16}O and ^{18}O kinematic scattering factors. The ^{18}O peak intensity is also scaled by the ratio of scattering cross sections for the two O isotopes (this ratio is very close to 1). The spectra are given for the scattering angle of 133°, which provides a better energy separation of the peaks originating from different oxygen isotopes. The fact that the two O peaks have the same height indicates that there is a uniform isotopic intermixing in the nearly equal proportions in the bulk of the film. The width of the ^{16}O peak is somewhat larger than that of the ^{18}O peak. We conclude that the ^{16}O distribution is broader and is characterized by a deeper penetration into the substrate. The interfacial SiO_2 layer grown during reoxidation is mostly formed by the ^{16}O isotope initially present in the film. This could not be realized if oxygen from the gas phase was able to migrate directly to the interface via interstitial diffusion; instead, it is transported across the film by an exchange mechanism with network oxygen in the silicate.

A second sample was annealed in vacuum at a lower temperature (400 °C), corresponding to the unchanged spectrum in Fig. 3, which contains a significant amount of CeO_2. As with the first sample, this film was then exposed to 10^{-2} Torr $^{18}O_2$ for 15 min at 500 °C. Figure 4(b) shows the difference between the spectra before and after reoxidation for this sample compared to the difference spectra for the silicate film shown in Fig. 4(a). This type of data presentation conveniently describes the ^{18}O incorporation (^{18}O portion of the spectra), loss of the oxygen from the film (negative fraction of the ^{16}O peak), and inward oxygen diffusion (positive fraction of the ^{16}O peak). For Hf (and Zr) based systems, an increase of the SiO_2 concentration in silicate composition results in slower oxygen transport and reduced reaction rates of oxygen with a film.[40] Increasing the SiO_2 fraction x in $HfO_2(SiO_2)_x$ from 0 (pure hafnium oxide) to $x=1$ (hafnium silicate) results in a reduction of the ^{18}O gain during reoxidation to an essentially negligible value. The behavior is different for the cerium silicate, however. As seen from Fig. 4(b), there is only a small difference in oxygen behavior for the two films. A slightly higher ^{18}O uptake is observed for the silicate, quite different from the strong suppression of oxygen incorporation in hafnium silicate films. Essentially all Ce species in the silicate film are in the incompletely oxidized 3+ state, while the cerium oxide film contains Ce^{4+}. That could contribute to easier oxygen incorporation into the cerium silicate by means of Ce oxidation into 4+ state and its subsequent reduction to Ce^{3+} by Si oxidation. Also, the SiO_2 interfacial layer, initially present in the film containing CeO_2 and not found in the silicate film, makes oxygen reaction with substrate Si more difficult in the case of the CeO_2 film.

IV. CONCLUSIONS

We have studied cerium oxide films on Si(100) using MEIS, XPS, and AFM. The as-deposited films consisted of ~40 Å thick cerium oxide and silicate over an ~10 Å silica-covered substrate as determined by XPS and MEIS. Vacuum annealing these films to 750 °C readily converted the cerium oxide to cerium silicate. Thermal stability and composition studies on the oxide and silicate films were performed using MEIS under several annealing conditions and upon reoxidation in $^{18}O_2$ gas. Finally, we have studied the film morphology before and after annealing using AFM.

Under the conditions of this study, the films grew with slablike morphology, with the Si substrate covered with, in order, silica:silicate:ceria, a metastable structure, with the relative thickness of the more stable silicate layer controlled by temperature and time. The oxygen isotopic MEIS analysis showed that oxygen transport in both the ceria and cerium silicate films happens via an exchange mechanism, although at different rates. Upon reoxidation of the cerium oxide and silicate films, the SiO_2 formation is more pronounced than in the hafnium oxide and hafnium silicate cases, where only O exchange in the bulk of the film occurs under similar oxidation conditions. Converting the ceria films into a silicate by vacuum annealing did not result in a significant change in the O reaction rate: this can be attributed to (1) a larger concentration of the Ce^{3+} species that are quick to react with oxygen and (2) a thinner interfacial SiO_2 barrier layer (resulting from mixing into silicate upon annealing) in the silicate film as compared to the oxide. In addition, AFM results show that the films remain flat under the annealing conditions used here until they decompose.

Our MEIS data show that annealing the films in vacuum produces a cerium silicate film with a sharp silicon-silicate interface: the complex silicate films that resulted from vacuum annealing possessed no interfacial silicon oxide layer (presumably limited by the total oxygen content in the overlayer). Studying these cerium silicate films for high-k device applications could be promising, but a careful study to electrically characterize the silicate films is needed. We suggest that it is possible to control the oxygen content in

these films; the composition is strongly a function of temperature and oxygen exposure, so fine tuning the films' stoichiometry for engineering applications appears possible. While a more detailed study may well show a more complex behavior, our AFM data to date indicate that the films remain reasonably flat during heating to 750 °C.

ACKNOWLEDGMENTS

The authors are grateful to Dr. P. Lysaght for useful discussions. This work was supported by the SRC/Sematech FEP and NSF (DMR 0218406).

[1]A. I. Kingon, J.-P. Maria, and S. K. Streiffer, Nature (London) **406**, 1032 (2000).
[2]G. D. Wilk, R. M. Wallace, and J. M. Anthony, J. Appl. Phys. **89**, 5243 (2001).
[3]K. J. Hubbard and D. G. Schlom, J. Mater. Res. **11**, 2757 (1996).
[4]Y. Nishikawa, N. Fukushima, N. Yasuda, K. Nakayama, and S. Ikegawa, Jpn. J. Appl. Phys., Part 1 **41**, 2480 (2002).
[5]T. Ami and M. Suzuki, Mater. Sci. Eng., B **54**, 84 (1998).
[6]T. Ami, Y. Ishida, N. Nagasawa, A. Machida, and M. Suzuki, Appl. Phys. Lett. **78**, 1361 (2001).
[7]H. W. Song, C. S. Lee, D. G. Kim, and K. No, Thin Solid Films **368**, 61 (2000).
[8]A. H. Morshed, M. E. Moussa, and S. M. Bedair, Appl. Phys. Lett. **70**, 1647 (1997).
[9]W. C. Choi, H. N. Lee, E. K. Kim, Y. Kim, C.-Y. Park, H. S. Kim, and J. Y. Lee, Appl. Phys. Lett. **75**, 2389 (1999).
[10]B. Hirschauer, M. Gothelid, E. Janin, H. Lu, and U. O. Karlsson, Appl. Surf. Sci. **148**, 164 (1994).
[11]E. J. Preisler, O. J. Marsh, R. A. Beach, and T. C. McGill, J. Vac. Sci. Technol. B **19**, 1611 (2001).
[12]T. Inoue, Y. Yamamoto, S. Koyama, S. Suzuki, and Y. Ueda, Appl. Phys. Lett. **56**, 1332 (1990).
[13]T. Chikyow, S. M. Bedair, L. Tye, and N. A. El-Masry, Appl. Phys. Lett. **65**, 1030 (1994).
[14]J.-H. Yoo, S.-W. Nam, S.-K. Kang, Y.-H. Jeong, D.-H. Ko, J.-H. Ku, and H.-J. Lee, Microelectron. Eng. **56**, 187 (2001).
[15]L. Kim, J. Kim, D. Jung, C.-Y. Park, C.-W. Yang, and Y. Roh, Thin Solid Films **360**, 154 (2000).
[16]J. Kang, X. Liu, G. Lian, Z. Zhang, G. Xiong, X. Guan, R. Han, and Y. Wang, Microelectron. Eng. **56**, 191 (2001).
[17]R.-P. Wang, S.-H. Pan, Y.-L. Zhou, G.-W. Zhou, N.-N. Liu, K. Xie, and H.-B. Lu, J. Cryst. Growth **200**, 505 (1999).
[18]J. F. Kang, G. C. Lian, Y. Y. Wang, and R. Q. Han, Solid State Commun. **108**, 225 (1998).
[19]T. Inoue, T. Ohsuna, L. Luo, X. D. Wu, C. J. Maggiore, Y. Yamamoto, Y. Sakurai, and J. H. Chang, Appl. Phys. Lett. **59**, 3604 (1991).
[20]B. Hirschauer, M. Goethelid, M. Davila, and U. O. Karlsson, Surf. Sci. **464**, 117 (2000).
[21]F. U. Hillebrecht, M. Ronay, D. Reiger, and F. J. Himpsel, Phys. Rev. B **34**, 5377 (1986).
[22]E.-E. Latta and M. Ronay, J. Vac. Sci. Technol. A **4**, 1626 (1986).
[23]T. Inoue, Y. Yamamoto, and M. Satoh, Thin Solid Films **343–344**, 594 (1999).
[24]T. Inoue, Y. Yamamoto, and M. Satoh, J. Vac. Sci. Technol. A **19**, 275 (2001).
[25]Y. W. Beag, K. Egawa, and R. Shimizu, Rev. Sci. Instrum. **64**, 3647 (1993).
[26]T. Gustafsson, H. C. Lu, B. W. Busch, W. H. Schulte, and E. Garfunkel, Nucl. Instrum. Methods Phys. Res. B **183**, 146 (2001).
[27]W. H. Schulte, B. W. Busch, E. Garfunkel, T. Gustafsson, G. Schiwietz, and P. L. Grande, Nucl. Instrum. Methods Phys. Res. B **183**, 16 (2001).
[28]J. F. van der Veen, Surf. Sci. Rep. **5**, 199 (1985).
[29]G. Moliere, Z. Naturforsch. A **2A**, 133 (1947).
[30]H. H. Andersen and J. F. Ziegler, *Hydrogen Stopping Powers and Ranges in All Elements* (Pergamon, New York, 1977), Vol. 3.
[31]W. K. Chu, Phys. Rev. A **13**, 2057 (1976).
[32]Q. Yang, D. J. O'Connor, and Z. Wang, Nucl. Instrum. Methods Phys. Res. B **61**, 149 (1991).
[33]A. Fujimori, Phys. Rev. B **27**, 3992 (1983).
[34]A. Fujimori, Phys. Rev. B **28**, 2281 (1983).
[35]A. Fujimori, Phys. Rev. B **28**, 4489 (1983).
[36]J. F. Ziegler and J. P. Biersack, SRIM, the stopping and range of ions in matter, Version 9, IBM, 1998.
[37]J.-P. Maria, D. Wicaksana, A. I. Kingon, B. Busch, H. Schulte, E. Garfunkel, and T. Gustafsson, J. Appl. Phys. **90**, 3476 (2001).
[38]H. Watanabe and N. Ikarashi, Appl. Phys. Lett. **80**, 559 (2002).
[39]B. W. Busch, W. H. Schulte, E. Garfunkel, T. Gustafsson, W. Qi, R. Nieh, and J. Lee, Phys. Rev. B **62**, R13290 (2000).
[40]D. Starodub (unpublished).